NASA Technical Memorandum 104262

Stratospheric Turbulence Measurements and Models for Aerospace Plane Design

L.J. Ehernberger

December 1992

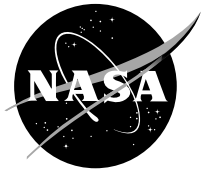

National Aeronautics and
Space Administration

NASA Technical Memorandum 104262

Stratospheric Turbulence Measurements and Models for Aerospace Plane Design

L.J. Ehernberger
NASA Dryden Flight Research Facility
Edwards, California

1992

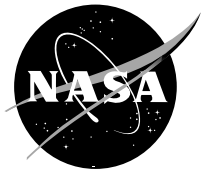

National Aeronautics and
Space Administration

Dryden Flight Research Facility
Edwards, California 93523-0273

STRATOSPHERIC TURBULENCE MEASUREMENTS AND MODELS FOR AEROSPACE PLANE DESIGN

L.J. Ehernberger*
NASA Dryden Flight Research Facility
P.O. Box 273
Edwards, California 93523-0273

Abstract

Progress in computational atmospheric dynamics is exhibiting the ability of numerical simulation to describe instability processes associated with turbulence observed at altitudes between 15 and 25 km in the lower stratosphere. As these numerical simulation tools mature, they can be used to extend estimates of atmospheric perturbations from the present gust database for airplane design at altitudes below 15 km to altitudes between 25 and 50 km where aerospace plane operation would be at hypersonic speeds. The amount of available gust data and number of temperature perturbation observations are limited at altitudes between 15 and 25 km. On the other hand, in-situ gust data at higher altitudes are virtually nonexistent. The uncertain potential for future airbreathing hypersonic flight research vehicles to encounter strong turbulence at higher altitudes could penalize the design of these vehicles by undue cost or limitations on performance. Because the atmospheric structure changes markedly with altitude, direct extrapolation of gust magnitudes and encounter probabilities to the higher flight altitudes is not advisable. This paper presents a brief review of turbulence characteristics observed in the lower stratosphere and highlights the progress of computational atmospheric dynamics that may be used to estimate the severity of atmospheric transients at higher altitudes.

Nomenclature

CAT	clear air turbulence
Fr	Froude number, N_{F_r}
g	acceleration caused by gravity, m/sec^2
h	geopotential altitude, km
$\dot{h}$	rate of change of altitude, m/min
HAT	high-altitude turbulence
HICAT	high-altitude clear air turbulence
L	height of the flow barrier in the Froude number
MSL	mean sea level
p	pressure, mb
PSD	power spectral density
rms	root mean square
T	temperature, K
U	horizontal windspeed component
U_{de}	derived equivalent gust velocity
$\ddot{U}$	second derivative of U with respect to altitude
USAF	United States Air Force
w	vertical velocity component
x	horizontal coordinate
β	atmospheric static stability parameter, $g\delta\theta/\theta\delta h$
δ	derivative operator
Δ	finite difference operator
θ	potential temperature, $T(1000/p)^{0.286}$
ρ	atmospheric density

Introduction

Advanced hypersonic research vehicles, such as the National Aero-Space Plane, require discrete atmospheric perturbation models for design at altitudes above the present gust and turbulence design criteria based on in-situ measurements. Recent developments indicate that numerical simulation of small-scale atmospheric dynamics could assist in the specification of these discrete

*Associate Fellow, AIAA.

atmospheric perturbation models for hypersonic aircraft design, especially at high flight altitudes. The atmospheric turbulence environment specified for design of civil and military aircraft is described as a function of altitude in terms of discrete and random gust inputs.[1–2] These discrete inputs are given as the derived equivalent gust velocity.[3]

Continuous random inputs are specified by a power spectral density (PSD) shape, wavelength scale factor, and root-mean-square (rms) value.[4] These design data are based on extensive gust loads surveys aboard operational aircraft and on true gust velocity measurement programs on specially instrumented military and research aircraft.[5–8] The adequacy of these criteria for gust loads design of subsonic aircraft to altitudes of approximately 15 km has been demonstrated on narrow- and wide-body transport aircraft.[5] For the higher altitudes, gust loads and true gust velocity data have been obtained by U-2 aircraft (Lockheed Corporation, Burbank, California) to altitudes of approximately 20 km.[9–10] These data have also been obtained by supersonic research aircraft to altitudes of 25 km.[11–14]

Because hypersonic flight research will use altitudes to approximately 50 km, these existing in-situ atmospheric turbulence data cover approximately one-half of the altitude range required. Moreover, subsonic transport airplane design has emphasized gust input effects on the limit load and fatigue life design. In contrast, hypersonic vehicles are more likely to require emphasis on propulsion and flight control systems responses. Response of hot structures to high-altitude turbulence and gusts will also be required. In flight regimes where more than one system is sensitive to the perturbation inputs, the interacting responses will probably involve more than one of the input perturbation components. For example, critical responses may simultaneously involve vertical and horizontal gust components as well as combinations of gust velocity and ambient density or temperature. In this regard, a chief limitation of the present gust database and design criteria is that they have only been established for single, independent perturbation component inputs. That is, for present conventional aircraft design, combinations of vertical and horizontal gusts are prescribed as being statistically independent. In addition, present aircraft design criteria do not link either the horizontal or vertical gust components with perturbations in temperature, density, or pressure.

These concerns for hypersonic aircraft design apply not only to the present database altitudes below 25 km but also become even more critical at altitudes from 25 to 50 km where higher speed airbreathing aerodynamic flight will be pioneered. Thus, two major aspects of the turbulence environment remain to be explored for hypersonic aircraft. The first aspect is statistical characterization of the intensity and amount of turbulence throughout the stratosphere. The second aspect involves description of the nature of coupling between gust motion components and pressure, density, and temperature state perturbations. Formulation of higher altitude design criteria and perturbation models addressing both of these aspects requires use of advanced numerical simulation techniques for small-scale atmospheric perturbations. In addition, appropriate observations to validate the simulations for these applications are needed.

This paper provides a brief overview of the characteristics of turbulence observed in the lower stratosphere. Current studies for the use of small-scale, two-dimensional, numerical atmospheric dynamics simulations for specification of the higher altitude perturbation environment are also discussed. Finally, a simple, generic, discrete atmospheric perturbation model proposed for assessment of hypersonic aircraft sensitivity to combinations of atmospheric gusts and thermodynamic transients is described.

Metric units have been used throughout this paper. For the convenience of readers who are more familiar with the U.S. Customary System, conversion factors are as follows:

U.S.	Metric	Conversion factor
Celsius, °C	Kelvin, K	°C = K – 273.15
Fahrenheit, °F	Kelvin, K	K = (5⁄9)(°F + 459.67)
Feet, ft	Meters, m	m = ft × 0.3048
Millibar, mb	Hectopascal, hPa	mb = hPa
Nautical miles, n. mi.	Kilometers, km	n. mi. = km × 0.54

Grateful appreciation is extended to the following collaborating researchers: Dale Durran, University of Washington, Seattle, Washington; Terry Clark, National Center for Atmospheric Research, Los Angeles, California; and Morton Wurtele and his team at the University of California, Los Angeles, California. Support for this work from NASA through NCC 2-374 and from the National Aero-Space Plane Program is also gratefully acknowledged.

Atmospheric Structure

Figure 1 shows the atmospheric layers with respect to the average January conditions at Edwards, California. These data are based on rawinsonde observations to

30-km altitude and nearby rocketsonde data for altitudes from 30 to 70 km and serve as a representative example of midlatitude winter conditions.[15] In the troposphere, temperature generally decreases about 6.5 K/km altitude, and windspeed generally increases up to the tropopause level at the base of the stratosphere. In the lower stratosphere, temperature tends to be nearly constant with altitude (isothermal), and windspeed generally decreases to minimum values at altitudes between 20 or 25 km. In the upper stratosphere, the rate of temperature increase reaches approximately 2.8 K/km. Windspeeds increase with altitude through the upper stratosphere into the mesosphere, where the temperature again decreases at rates of 2 to 4 K/km altitude. The division between the stratosphere and mesosphere is termed the *stratopause*.

In the lower troposphere, sensible heat is actively exchanged by mixing processes which bring air into contact with the earth and sea surfaces. Low altitude warming predominates during the day at lower latitudes. Conversely, cooling prevails at night and at higher latitudes. Much heat is also exchanged throughout the troposphere by moisture phase changes. Solar radiative heat input to the atmosphere is located predominantly in the upper stratosphere where chemical species, such as ozone, absorb solar ultraviolet radiation. Between these two heat source regions, temperatures are cooler in the upper troposphere and lower stratosphere. Basically, all atmospheric layers are subject to infrared radiative heat loss which, at the surface, may be notably limited by cloud cover.

Because air is compressible, temperature changes experienced by atmospheric airparcels are not limited to heat gain or loss. These changes are also affected by adiabatic expansion and compression when airparcels rise and descend. As airparcels are displaced adiabatically, that is, without heat gain or loss, up or down in the atmosphere, the temperatures change by a rate of nearly 10 K/km of altitude displaced. Cooling occurs for upward displacements, and warming results from downward displacements. Thus when vertical motion is not uniformly distributed in the atmosphere, airparcels with the most relative displacement experience the greatest temperature differences from the surrounding airmass. Subsequently as rising airparcels become cooler and more dense than the surrounding airmass, the force of gravity causes buoyancy effects to restore the airparcels toward their original altitude levels. Conversely, as descending airparcels become warmer or less dense than the surrounding ambient air, these parcels also experience restoring buoyancy which forces them toward their original altitude.

Because ambient temperatures increase with altitude in the stratosphere, the airparcel temperature contrast grows at rates of 10 to 13 K/km displaced, causing the buoyancy forces to act as a stiff spring. In comparison, weaker spring force effects are experienced in the troposphere and mesosphere, where airparcel temperature contrast grows at rates from 4 to 8 K/km displaced. This effect, in which airparcel altitude displacements are opposed by buoyancy forces, is much stronger in the stratosphere than in either the troposphere or the mesosphere. As a result, the term stratosphere is quite appropriate for this deeply stratified region of the atmosphere. The differences between wind and temperature structure in the troposphere and stratosphere also lead to inherent differences in atmospheric turbulence characteristics. Differences in turbulence characteristics are believed to include gust magnitudes, length scales, horizontal and vertical patch dimensions, patchiness or spacing between patches, and characteristics of associated temperature perturbations. As indicated in the next section, these characteristics have only been partially observed to date.

Turbulence Observations in the Lower Stratosphere

Early operation of the U-2 airplane in the 1950's provided gust loads data to altitudes near 23 km over several representative areas of the world.[9] The USAF High-Altitude Clear Air Turbulence (HICAT) Program subsequently conducted true gust velocity measurements in the stratosphere with the U-2 airplane over various terrain and geographical areas.[10] The XB-70 (North American Rockwell, Los Angeles, California) and YF-12 (Lockheed Corporation, Burbank, California) prototype supersonic cruise aircraft also provided high-altitude gust acceleration data and true gust velocity measurements as a part of aeronautical flight research programs.[11–14]

Results from these flight programs (fig. 2) generally indicate that the amount of turbulence expressed as a percentage of total flight distance decreases from a maximum near the jetstream and tropopause altitudes to a minimum near altitudes of 20 or 25 km. Figure 2 shows that the fraction of miles in clear air turbulence (CAT) for use with PSD criteria also decreases significantly in the lower stratosphere.[7] The altitudes at which the amount of turbulence decreases most changed somewhat from one sampling program to another. Presumably, these changes in the altitude of turbulence decrease were caused by seasonal differences in the atmospheric structure as well as geographical area.[13]

The number of gust loads or normal acceleration peaks cumulated from large to small and experienced as a function of overall flight distances also decreases dramatically (fig. 3) at the higher altitudes of the

supersonic airplane data. The cross-hatched area on fig. 3 shows that the range of gust loads acceleration experience for subsonic transport jet aircraft is close to the supersonic aircraft experience at altitudes between approximately 12 to 17 km. In contrast at altitudes above 18 km, gust accelerations experienced in supersonic flight are markedly less than those experienced in either subsonic or supersonic flight at lower altitudes. Because 25 km is generally near the altitude of minimal windspeed, gust loads are expected to remain relatively mild at altitudes between 20 to 25 km. At higher altitudes, however, winds generally increase although the direction may reverse. Such changes in windspeed indicate that the amount and intensity of turbulence may be expected to increase at altitudes of 30 to 50 km in the upper stratosphere.

Some insight into the observed decrease in turbulence at altitudes in the lower stratosphere is provided by inspection of seasonal trends, geographical patterns, and empirical associations with attending meteorological features. Figure 4 shows the seasonal variation in the relative amount of turbulence encountered in the lower stratosphere by the YF-12 airplane on flights made from Edwards, California.[13] These data are smoothed by a 3-month moving mean for the altitude layer from 12 to 17 km in the lower stratosphere. They depict a maximum in the winter and early spring when lower altitude jetstream and airmass frontal activity is greatest and a minimum in the summer and early fall when the winds in the lower stratosphere are weak and have reversed to easterlies.[15]

Meteorological Features of Turbulence in the Lower Stratosphere

On individual days, meteorologists have noted the association of high-altitude turbulence (HAT) at altitudes above 12.5 to 25 km with mountain-wave activity and strong winds blowing over the tops of large cumulonimbus clouds.[10,16–17] The association with wave activity was examined further for several of the XB-70 turbulence encounter days.[18–19] These findings not only supported the indications from studies by HICAT meteorologists[10,17] but also demonstrated the association of HAT with both rawinsonde balloon rise rates and with a parameter important to mountain-wave behavior, that is, the curvature of the lower altitude wind profile. Nominal rawinsonde balloon rise rates are typically from 250 to 300 m/min. These nominal rise rates may change gradually with balloon material characteristics, amount of inflation, and atmospheric temperature. Variations around the nominal rise rate will sometimes occur as a result of up- or down-drafts associated with cloud or wave activity in the atmosphere.

Large and cyclic variations in the balloon rise rates are indicative of mountain waves and turbulence encountered in the stratosphere.[18] Examples of the balloon rise rate variations associated with high-altitude turbulence conditions are shown by the profiles in Figs. 5(a) to (d).[18] These profiles represent two balloon ascents for a day with mountain-wave conditions and HAT and two ascents for another day with neither mountain waves nor HAT. For HAT cases, nearby balloon rise rate variations in the troposphere are generally in the range of 50 to 150 m/min. Nonturbulent cases generally have rise rate variations from 30 to 70 m/min. This study encompassed 112 balloon ascents from 7 locations over 39 high-altitude flight days. The criteria for large and cyclic balloon rise rate variations correctly indicated 80 percent of the HAT encounters on these days.

Another parameter associated with HAT is an increase in the wind profile curvature between altitudes from 3 to 7.6 km. Curvature is the second derivative of windspeed, $\ddot{U}/U$, with respect to altitude divided by windspeed. A curvature increase between two altitudes ($\Delta\ddot{U}/U > 0$) is conducive to the formation of large amplitude mountain waves.[19] These findings were developed by identifying areas of expected mountain-wave activity and those with positive curvature parameter changes in the lower troposphere between layers centered near 3 and 7.6 km and examining these areas with respect to turbulence encountered along the flight track of the XB-70 airplane (Fig. 6). For evaluation of the forecast, skills provided by the curvature parameter nonturbulence regions were also specified in smooth areas of the flight track where altitude changes were minimal. The flight example shown in Fig. 6 has two HAT encounters in areas of expected mountain-wave activity where the curvature criteria were fulfilled, one smooth segment of the track in another area of expected wave activity, and four smooth track segments which were outside of these areas. Overall evaluation of this forecast parameter on 15 high-altitude flights resulted in correct identification of 40 turbulence encounters out of a total of 47 encounters and one false alarm in 43 nonturbulence areas. Thus, the role of lower altitude wave activity has been empirically established by independent investigators for a significant portion of HAT cases encountered by both subsonic and supersonic aircraft. This finding was significant but not surprising because mountain waves had been known to increase the severity of CAT at passenger jet cruise altitudes. Many researchers have been instrumental in the analysis and demonstration of CAT enhancement by mountain-wave-induced vertical displacement of shear layers to cause Kelvin-Helmholtz wave amplification and instability.[20–25]

These convincing demonstrations of the Kelvin-Helmholtz instability role in CAT were undoubtedly a large part of the answer to explaining the generation of many CAT encounters. However, the Kelvin-Helmholtz instability explanations did not suffice as a large part of the solution to the CAT forecast and avoidance problem because its application would rely on forecasting the vertical displacement of windshear layers. Accurate forecasts of windshear layer displacements with the necessary detail in time and space are not feasible. The related atmospheric processes often involve such local phenomena as mountain waves with small-scale atmospheric variations which entail subgrid phenomena. None the less, mountain-wave field studies and theoretical analyses of the attending atmospheric dynamics have made considerable progress in the concepts of mountain-wave propagation behavior.[26–28]

An example of upward propagating mountain-wave activity which causes turbulence in the lower stratosphere is depicted by the temperature and wind fields analyzed for a case of in-situ aircraft observations in Fig. 7.[28] Moderate and severe turbulence was encountered at several aircraft sampling altitudes as denoted by the "hats" in the figure. Potential temperature is the temperature that the airparcel would have if adiabatically compressed to 1000 mb, that is, approximately 100 m mean sea level (MSL) pressure altitude. In Fig. 7, potential temperature contours are denoted by solid lines. Horizontal wind contours (isotachs, lines of constant speed) are shown as dashed lines. Upstream windspeeds exceed 60 m/sec near 7.5- and 12-km altitudes. At higher altitudes, the upstream winds generally decrease to less than 20 m/sec at 20-km altitude. The potential temperature contours, which approximate trajectory streamlines, show the downslope winds over the mountain ridge. Successive wave crests indicate partially trapped wave components at 5 to 7 km in the middle troposphere.

Although wave amplitudes are diminished near 11 km, a large amplitude jump is generated at the 14- to 17-km level. At 16-km altitude, upstream of the jump, the zero isotach indicates a narrow region of flow reversal. Such reversals suggest that cooler, more dense air from lower altitudes has been brought above warmer air to form a local layer of convective overturning. Unfortunately, the measurement scale was not sufficiently detailed to indicate the cell sizes of instabilities involved in this region. Strong horizontal temperature gradients are noted in the jump and downstream of the peak. At 16 km, the horizontal windspeed increases from less than zero in the blocked or overturning region to 40 m/sec in the peak of the jump. The windspeed then decreases to between 20 and 30 m/sec in a pronounced horizontal temperature gradient with strong turbulence. Near 19 km, the highest measurement altitude, light turbulence was still observed, and wave amplitudes and wavelengths were decreased. Wave cases are seldom identical and often change measurably over periods of an hour or more. Just the same, the features of this case are representative of wave character changes from the lower troposphere to the tropopause and lower stratosphere when moderate and severe stratospheric turbulence occurs. Note that the sharp density changes resulting from strong temperature perturbations in similar cases are often on the order of 5 percent. Such changes would have measurable impacts on aerodynamic coefficients and propulsion system mass flow for an aerospace plane.

Numerical Simulation of Wave Propagation

Relevant progress in applying numerical simulation to atmospheric gravity wave propagation, particularly into the lower stratosphere, has been recently reviewed.[29] Several numerical simulation codes are now available and may have a role in advancing the quantitative understanding of small-scale perturbations observed in the lower stratosphere and in the prediction of disturbances at altitudes above the present airplane design criteria database.[30–33] Numerical techniques are particularly applicable to the study of perturbations in the lower stratosphere because quantitative treatment of mountain-wave behavior by closed form solution is limited to simple analytical profiles of wind and thermal structures and to small obstacles or flow barriers. Multiple layers must be used to represent the irregular atmospheric wind and temperature profiles frequently associated with most cases of strong turbulence. Because the juncture between the troposphere and stratosphere at the tropopause and jetstream level is also an inherent, first-order, atmospheric discontinuity, multiple layers are also involved for estimating the amplitude of waves propagating into the stratosphere. Therefore, it is appropriate to seek numerical solution techniques to adequately account for the influence of irregular temperature and wind profiles on mountain-wave propagation and turbulence in the stratosphere.

An initial experiment to ascertain the viability of numerical simulations for application to small-scale stratospheric perturbations is described in the next three subsections.[34] A brief overview of other related numerical simulation studies follows in a later section.

Intercomparison Cases

In this initial comparison experiment, observed cases of disturbances in the lower stratosphere were compared with numerical simulation codes having various

underlying physical assumptions, numerical formulations, and topographical representation schemes.[34] Simulation input consisted of the topographic or barrier description as the lower boundary and the upstream profiles of atmospheric temperature and wind as the input condition at every vertical gridline. This comparison experiment was initiated to identify differences between the numerical codes that would be important to applications in the stratosphere and to provide a practical assessment of the capability for specifying the atmospheric profiles and topography for the numerical simulation initial conditions in applied cases. Moreover, agreement between observation and models indicates the viability of using the numerical simulation models to specify perturbation characteristics at altitudes above available observations.

Six cases of documented in-situ wave observations in the stratosphere[27–28,35–37] were selected for the pilot project intercomparisons of simulations by the numerical codes.[30–33] These simulation codes can run without restrictions of linearity or hydrostatic equilibrium. Differences in these codes include treatment of compressibility, topographic representation, grid structure (fixed cartesian versus variable-grid resolution and orthogonal curvilinear), and viscid effects.

Three topographic reliefs relative to the barrier are represented by the following cases:

- Sierra-Nevada and White Mountains
- Rocky Mountain Continental Divide west of Denver, Colorado
- Rocky Mountain ridgeline east of Alamosa, Colorado

The Sierra-Nevada and White Mountains have lower terrain upstream than downstream. The Rocky Mountain Continental Divide has higher terrain upstream than downstream. The Rocky Mountain ridgeline has approximately the same terrain elevation upstream as it does downstream from the barrier.

All six cases had in-situ aircraft observations at multiple altitudes from the upper troposphere to 18 km in the stratosphere. In four cases, strong turbulence was encountered in the stratosphere. The other two cases exhibited well-established wave activity in the lower troposphere but did not report notable turbulence or wave activity above 14 km. In the atmospheric layer at and below the mountain ridge level altitude, the cases represent an inverse square root of the Froude number ($N_{F_r} = U{**}2/Lg$). These cases range from approximately 0.8 to 3.5 and, therefore, cover more than a narrow range of dynamic flow conditions near the topography. This application to the atmosphere differs slightly from the Froude number as conventionally used in hydrodynamics. Here, U is the windspeed upstream of a mountain ridge height, L, and the atmospheric stability ($g\beta$ or $g\delta\theta/\theta\delta h$) is used in place of g alone because of atmospheric buoyancy.[29] The analyzed atmospheric wind and temperature data for the wave propagation event depicted in Fig. 7 is an example of the in-situ data used for comparison with the numerical simulations for these cases.[28]

Case Preparation for Numerical Model Input

Upstream atmospheric wind and temperature profiles were prepared for input to the numerical models from routinely archived upper air network rawinsonde data and synoptic charts. Figures 8 and 9 show examples of the original upper air observations and the resulting temperature and wind input profiles. For the first stage of the intercomparisons, preparation of the input atmospheric profiles and topographic representation was accomplished independently from the numerical modeling. These atmospheric data were interpolated in time and space to give representative values of wind and temperature at 1-km altitude intervals. As suggested by the scatter of the observed data around the input profiles, this data value selection process was subjective with a tendency to produce constant wind shear and lapse rate layers over large altitude segments.

Topographic barrier descriptions for the simulation lower boundary condition were also specified by a three-way, subjective compromise among aircraft ground track, ridge layer wind direction, and topographic irregularities. These independently prepared input data were then given to the numerical modeling personnel at the Universities of Washington (Seattle) and California (Los Angeles) without identification of the dates or in-situ case observations. Implementation of these input data in the models and selection of grid resolution, time step, model domain, and output simulation times were not rigidly restricted. Instead, such decisions were left to the expert judgment of the individual modelers.

Preliminary Comparison Results

Results of the initial intercomparisons between simulations and observed wave and turbulence were highly encouraging.[34] As an example, Figs. 10(a) to (d) show the strong contrast between simulations produced for wave perturbation cases, with and without strong turbulence in the stratosphere, for the potential temperature and horizontal windspeed fields. All three models which simulated these two cases exhibited similar contrast between the one with and the one without turbulence in the stratosphere. This turbulence case simulation

corresponds to the in-situ measurement analysis shown in Fig. 7. The simulation replicates the diminished wave amplitudes near 11 km, potential temperature jump between 14 and 17 km, large horizontal windspeed changes at 16 km, and decreased wave amplitudes and wavelength above 19 km.

Preliminary assessment of the simulation results for the six cases was based on inspection of qualitative wave propagation features. The qualitative features included wave character in the troposphere, wave amplitude propagation behavior in the tropopause zone, and wave-breaking tendency indicative of turbulence in the lower stratosphere. Inspection of the analyzed aircraft observation data for the 6 cases yielded 15 of these qualitative features for evaluation of the initial outputs available from 2 models. For the 30 qualitative wave propagation features examined on the simulations, agreement was judged as good for 21, as fair for 4, and as poor for 5 of the evaluated features.

Quantitative comparison of amplitudes for the larger wave perturbations at the flight data altitudes were also assessed. Quantitative examination emphasized the predominant perturbation wave heights, vertical velocity, and windspeed changes. Magnitudes of these features were generally estimated from contour plots for the observed and the numerical model output data. More than 50 percent of the 92 comparisons agreed to within a factor of 2.[34] In judging the goodness of this agreement, the following factors were considered:

- Perturbation magnitudes vary by more than a factor of 2 between subjective turbulence intensity-rating categories.
- Aircraft measured perturbation magnitudes typically change by 10 to 100 percent for repeated data runs at given altitudes within a 3-hr period.
- Manual data extraction from contour presentations is not precise.
- Strong perturbations are not expected to be steady state in either the atmosphere or the numerical simulations.

In view of these considerations, the present intercomparison results are judged to be excellent and very encouraging for the application of numerical simulation to wave perturbation phenomena in the stratosphere.[34]

Further assessment will consider the sensitivity of the individual models and comparisons among them to the following parameters:

- Resolution and smoothing of topographic features as well as representation by grid blocks (restricted to horizontal and vertical surfaces) versus terrain-following constructions
- Computational grid resolution in horizontal and vertical space dimensions as well as in the time-step size
- Duration of the simulations in atmospheric time
- Resource requirements in terms of computer time, cost, and user expertise

These assessments will consider present and future applications which may include extension to altitudes above 50 km and finer grid resolutions to study the influence of shear layers with Kelvin-Helmholtz instability.

Related Wave Propagation Studies

Generation of atmospheric turbulence in the stratosphere is basically the result of buoyant imbalance and motion stresses much the same as in the lower atmosphere. In the troposphere, however, buoyant imbalance is frequently caused by heating of the ground or clouds, releasing of latent heat in condensation processes, mixing as winds blow over rough terrain, or strengthening of upper air wind and temperature gradients. In contrast, a larger portion of turbulence in the stratosphere is caused by wave processes triggered by mountains, cloud barriers, or irregular jetstream dynamics which amplify as they propagate upward. In the troposphere, vertical propagation of some wave energy is frequently prevented by airmass layers. These layers have negative or neutral static stability, that is, no buoyant restoring force. Propagation is also prevented by reflection caused by strong changes in windspeed with altitude on the underside of the jetstream or by significant directional shifts in the wind profile. As wave motion components which escape the aforementioned limitations propagate upward, amplitude and velocity perturbations of these components tend to grow approximately with the inverse square root of the density ratio between altitudes.[29,38] Thus, upward wave leakage amplifies until it generates its own instabilities or meets other limiting factors in the wind or temperature static stability profile.

Ground-based measurements and satellite observations are among methods used to gather evidence of wave amplification and instability with propagation to higher altitudes in the mesosphere and thermosphere.[39–41] The extremely low density at these altitudes leads to large amplitude disturbances which are observable by remote means. These phenomena are believed to explain much of the atmospheric density variations inferred from space shuttle entry trajectory data.[42] The most dramatic of these was the alleged “density hole” which strongly perturbed the Space Shuttle *Columbia* causing a jolting response similar to heavy turbulence during atmospheric entry near 76-km altitude on STS-4.

Most concern for airbreathing hypersonic flight research is, however, at much lower altitudes where dynamic pressures will be sufficient for acceleration and level cruise. Thus, the need for realistic specification of atmospheric perturbations for hypersonic flight is most critical at altitudes from 25 to 50 km. These altitudes are above the limit of most in-situ data, yet they are still somewhat below most of the remote observation studies.

The mechanisms involved in wave propagation from the middle stratosphere to the mesosphere have been studied by a limited number of numerical simulations which have required considerable computer time.[43] These simulation studies have illustrated the amplification and instability processes and have provided useful additions to conventional theoretical interpretations. As an example, Figs. 11(a) to (d) show the potential temperature contours resulting from a numerical simulation of wave propagation between altitudes of 30 and 50 km.[43] The wave response is triggered by a barrier located 50 km downstream from the inflow boundary and at the base altitude of the simulation, 30 km. The potential temperature contours, which approximate flow streamlines for nearly steady conditions, show the wave amplitude increases with altitude. At 10-hr simulation time (Fig. 11(a)), the upward motion becomes very steep in patches between 40- and 50-km altitude. In local regions where the potential temperature contours slant back to the left as they go up, the simulation produces colder, more dense air over warmer, lighter air. The prevailing left-to-right wind decelerates and begins to reverse. Continuation of this process (Figs. 11(b) and (c)) leads to further reversal of the wind in these local regions and to wave breaking or overturning as the small areas of cold air accelerate downward. Turbulence and mixing in these small areas develop regions of nearly constant potential temperature as noted by the tendency to form pockets of separated potential temperature isotherms (Fig. 11(c)) at 14 hr into the simulation. Finally at 16 hr (Fig. 11(d)), the wave perturbations and turbulence decay before the onset of another cycle of wave propagation, growth, and overturning.

In spite of the value of this upper stratosphere numerical simulation work, many questions of wave behavior remain to be answered in the lower stratosphere (below 30 km) before the knowledge of higher altitude wave behavior can contribute to design risk definitions for hypersonic vehicles. These questions involve the frequency of significant wave component generation at, or propagation through, the tropopause. The critical layer behavior in the lower stratosphere must also be ascertained. Studies of the instability zone associated with the critical level will greatly assist in this effort.

Wave propagation studies have recently addressed the lower stratospheric structure where wind decreases with altitude. Theoretically, critical levels occur where the windspeed equals the wave-phase speed (or zero windspeed for a standing wave). Results of this work emphasize the following facets of wave propagation behavior:

- Critical level behavior, wherein propagating wave energy is converted to turbulent and kinetic energy, is commonly manifested a few kilometers below the actual critical level altitude where the primary upward propagating wave meets reflected wave components which are propagating downward.[44]
- Critical level criteria do not need to be completely fulfilled to induce a layer of instability in the lower stratosphere.[45] That is, the windspeed decrease with altitude does not actually need to reach zero (or reverse) with respect to the wave.
- Because of the effects of Earth rotation, longer wavelength inertial-gravity wave propagation can induce instabilities at multiple levels over a broad or deep altitude zone depending on the atmospheric profile structure and mode wavelength or wave number.[29,45]
- Nonhydrostatic effects impact the momentum flux and cause wave perturbations in the stratosphere to occur further downwind than predicted by solutions based on the simplifying hydrostatic assumption.[46]

Figures 12(a) to (d) show an example from the previously cited studies.[44] This example depicts instability development in a deep layer of decreasing wind with an upward propagating wave component approaching the critical level. Wave propagation behavior in this simulation study corresponds to what may be expected in the altitude band from 15 to 30 km at times. In this case, the input upstream windspeed decreases with constant shear from 10 m/sec at 15 km (the base altitude of the layer) to 0 m/sec at 25-km altitude (the critical level) and continues in reverse direction to –5 m/sec at 30-km altitude. Figures 12(a) to (d) show the streamfunction resulting from monotonic excitation having a wavelength of 10 km and an amplitude less than 150 m introduced at the base altitude of 15 km of the nonlinear, spectral simulation. For clarity of illustration, Figs. 12(a) to (d) show the streamfunction patterns for only the 20- to 26-km altitude section of the simulation at times of 4, 9, 10, and 12 hr after introduction of the 10-km wave at the lower boundary. In addition to delineate the instability pattern, the streamfunction contour interval resolution is decreased by a factor of 10 just below the 22-km altitude.

The first phase, depicted in Fig. 12(a) at 4 hr into the simulation, shows the wave crests and troughs slope upstream with altitude as they propagate to higher altitudes. As the propagation process continues, critical level interactions reflect wave energy which modifies the form of the upward propagating wave. This interaction subsequently produces sloping zones of reverse flow at altitudes between 23 km and the critical level at 25 km as shown in Fig. 12(b) for 9 hr into the simulation. At this time, rapid development of smaller scale instabilities is initiated and becomes evident between altitudes of 22 and 24 km just 1 hr later as shown in Fig. 12(c). As the instability processes enter their later stages at 12 hr into the simulation time (Fig. 12(d)), note that the small-scale disturbances not only extend below 22 km but some also begin to propagate above the critical level at 25 km. This instability zone below the critical level, somewhat above the tropopause and jetstream altitudes, will often be at altitudes where airbreathing vehicles accelerate from supersonic to hypersonic speeds. This progress in numerical wave propagation and simulation studies indicates that atmospheric dynamics can have a greater role in the quantitative understanding of small-scale perturbations observed in the lower stratosphere and in the prediction of disturbances at altitudes above the present database for aircraft design criteria. The challenges and recommendations for further progress in the definition of strong discrete perturbations at stratospheric altitudes are clear. Meteorological observations and in-situ atmospheric data from the troposphere and lower stratosphere are required to provide the basic statistical characterization of perturbation activity at these levels. Definition of perturbations at higher altitudes requires numerical simulation of the upward propagation dynamics. Such definition would help in determining how these perturbations are affected by the atmospheric structure and under what meteorological conditions instabilities will result in strong perturbations and turbulence at higher altitudes. As numerical simulation studies progress, their realism can be evaluated in stages by comparison with in-situ perturbation measurements, with wave amplitude observations by rawinsonde balloon rise rate in the middle stratosphere, and with remotely detected wave activity in the mesosphere. Such work should significantly improve the accomplishment of two basic goals. These goals are as follows:

- To predict the nature of wave propagation and instabilities at higher altitudes
- To improve estimates of the perturbation-length scales and maximum magnitudes for hypersonic aircraft design purposes

These accomplishments will inherently support the definition of hypersonic vehicle design criteria and the formulation of simple, discrete models for characterizing perturbations in the vertical and horizontal wind components as well as the pressure, density, and temperature states.

Discrete Perturbation Model Concept

This section describes a simple, initial, generic concept for a combined discrete atmospheric perturbation model. Such models may be used for design sensitivity assessment. However, their use as design criteria throughout the stratosphere will not be warranted until the appropriate magnitudes, scale lengths, and risk levels are better estimated for the higher altitudes.

The traditional derived equivalent gust velocity, U_{de}, is basically a discrete perturbation form which has served its purpose well as an airframe lifetime gust loads predictor for altitudes which were surveyed with similar aircraft.[5] Its one-minus-cosine load shape, in which the gust encounter builds up in the positive direction and decays back to zero over a distance of 25 wing chord lengths, is a one-sided model for the vertical gust component alone. As airframe structures became more flexible, it became prudent to characterize gust data in terms of the turbulence PSD for the evaluation of second-order responses.[4] For some preliminary design studies, simple, repeatable inputs of sharp, two-sided transients which represent the larger magnitude perturbations embedded in continuous turbulence are desirable. Hypersonic vehicle airworthiness may depend on gust-induced responses for several subsystems, such as propulsion, flight control, and basic sensor capabilities, in addition to the gust loads on the structure. Therefore, the discrete perturbation model must include all physical components of the atmospheric transients that may affect the vehicle.

One simple, generic model that combines all of the perturbation variables is a vortex with solid body rotation in the core and velocity components outside the core decaying inversely with distance from the core. This perturbation form is generally characteristic of atmospheric observations for phenomena including vortex-ring segments accompanying downburst outflows, dust devils, and higher altitude rotor formation resulting from Kelvin-Helmholtz instability and other familiar vortex shedding phenomena.[21,47] Generation of the instability cells results from wave amplification which brings up colder, more dense air and brings down warmer, less dense air. Figure 13 shows potential temperature isotherm distortion leading to formation of a strong turbulent perturbation.

When vortex formation occurs with the axis of the core in the horizontal plane, the gust velocity component perpendicular to the flightpath achieves maximum perturbation velocity along trajectories through the center of the core. The perturbation component parallel to the flightpath attains maximum amplitude for trajectories tangential to the outer edge of the core. For illustration of the resulting perturbations, the maximum gust velocity of 10 m/sec with the vortex core radius dimensioned to 200 m is selected. This combination of maximum gust velocity and core radius produces an arbitrarily strong maximum shear of 0.05 sec^{-1}.

Figure 14(a) shows the vertical gust velocity for a horizontal flight trajectory through the center of the core. In comparison, note that the peak-to-peak perturbation amplitude through the core is approximately the same as prescribed for maximum cruise speed at 15 km.[1] The horizontal component for this trajectory directly through core center of the idealized perturbation does not experience any variation. Both horizontal and vertical components experience comparable perturbation magnitudes for horizontal trajectories through the upper or lower edges of the core.

Figure 14(b) illustrates the horizontal and vertical components of the discrete perturbation model for a trajectory tangential to the (that is, through the) upper edge of the core. Again, note that the amplitudes of this discrete model are approximately the same as the Ref. 1 criteria for design loads criteria at maximum dive speed at an altitude of 15 km. For the temperature change, a value of 10 K with buildup and drop-off distances of 400 m is used. This value appears to be reasonably conservative on the basis of previously reported aircraft measurements.[48] Because temperature transient peaks often do not coincide with peaks in the gust velocity components, the coldest temperature is offset 200 m to the updraft side of the core as illustrated with the attending ambient density variation in Fig. 14(c). This configuration of cold air relative to the motion components is highly arbitrary because neither the most prevalent nor the most critical patterns are known. Pressure is approximated by use of Bernoulli's equation and the equilibrium assumption that the pressure gradient force balances the centrifugal force. For this model, the pressure perturbation is less than 0.1 percent at the outer edge of the core. This perturbation is not illustrated because it results in a nearly negligible effect on density.

Specification of such simple, discrete perturbation models as well as their geometric dimensions and perturbation magnitudes is reasonably straightforward for the altitudes of available in-situ data below approximately 20 km. At higher altitudes above available in-situ data, selection of the gust and thermodynamic perturbation magnitudes as well as the appropriate geometric length scales becomes highly questionable. Discrete perturbation model specification for hypersonic aircraft design at these higher altitudes requires the use of numerical simulation of the small-scale dynamic atmospheric processes which lead to strong perturbations in gust velocities, temperature, and density.

Concluding Remarks

Vehicle design criteria for lower altitudes have served their purpose well for structural design of subsonic aircraft to altitudes of approximately 15 km. However, these criteria do not incorporate combined perturbation inputs for either the motion components or the temperature, pressure, and density states. These states are expected to be more significant to airbreathing hypersonic vehicles. In addition, the amount of in-situ data for establishing gust design criteria decreases markedly between altitudes of 15 and 25 km. Above these altitudes, essentially no in-situ data have been gathered. Available data for turbulence and temperature transients encountered by aircraft in the lower stratosphere often show an association with lower altitude mountain-wave activity. Therefore, improved understanding of upward wave propagation processes is a key element in the formulation of atmospheric perturbation design criteria for higher altitude aircraft.

Recent advances in numerical simulation of wave propagation processes are making such improvements in understanding the conditions and atmospheric structures associated with the development of wave instabilities which cause turbulence and strong gusts. A current experiment comparing in-situ observations of mountain-wave-induced perturbations in the lower stratosphere with two-dimensional, numerical, atmospheric dynamics simulations made by separate codes was described. Initial results from these comparisons indicate numerical simulations will provide useful descriptions of higher altitude perturbations. An example of a simple, generic, discrete perturbation model combining motion components and thermodynamic (pressure, density, and temperature) disturbances was given. Definition of appropriate disturbance magnitudes and length (dimensional) scales for such discrete atmospheric perturbation models at altitudes of 25 to 50 km is needed for hypersonic vehicle design. These perturbation magnitudes and length scales can be defined by studies which combine these numerical atmospheric simulation tools with higher altitude observations in the middle and upper stratosphere.

References

[1] U.S. Dept. of Transportation, Federal Airworthiness Regulations, *Airworthiness Standards: Transport Category Airplanes*, pt. 25, app. G, change 19, 1974.

[2] USAF, Military Specification, *Airplane Strength and Rigidity Flight Loads*, MIL-A-8861B, Feb. 1986.

[3] Pratt, Kermit G. and Walker G. Walker, *A Revised Gust-Load Formula and a Re-Evaluation of V-G Data Taken on Civil Transport Airplanes From 1933 to 1950*, NACA-1206, 1954.

[4] Houbolt, John C., Roy Steiner, and Kermit G. Pratt, *Dynamic Response of Airplanes to Atmospheric Turbulence Including Flight Data on Input and Response*, NASA TR R-199, 1964.

[5] Zalovcik, J.A., J.W. Jewel, Jr., and G.J. Morris, *Comparison of VGH Data From Wide-Body and Narrow-Body Long-Haul Turbine-Powered Transports*, NASA TN D-8481, 1977.

[6] Rhyne, Richard H. and Roy Steiner, *Power Spectral Measurement of Atmospheric Turbulence in Severe Storms and Cumulus Clouds*, NASA TN D-2469, 1964.

[7] Hasty, Paul L., *A Description of the Atmospheric Turbulence Environment Derived From the Critical Atmospheric Turbulence (ALLCAT) Program*, AFFDL-TR-77-4, 1977.

[8] Murrow, Harold N., "Measurements of Atmospheric Turbulence," *Atmospheric Turbulence Relative to Aviation, Missile, and Space Programs*, NASA CP-2468, 1986, pp. 73–92.

[9] Coleman, Thomas L. and Roy Steiner, *Atmospheric Turbulence Measurements Obtained From Airplane Operations at Altitudes Between 20,000 and 75,000 Feet for Several Areas in the Northern Hemisphere*, NASA TN D-548, 1960.

[10] Crooks, Walter M., Frederic M. Hoblit, Finis A. Mitchell, et. al., *Project HICAT—High Altitude Clear Air Turbulence Measurements and Meteorological Correlations*, AFFDL-TR-68-127, vol. I, 1968.

[11] Wilson, Ronald J., Betty J. Love, and Richard R. Larson, *Evaluation of High-Altitude Turbulence Encounters on the XB-70 Airplane*, NASA TN D-6457, 1971.

[12] Reukauf, Paul J., Frank V. Olinger, L.J. Ehernberger, and Craig Yanagidate, "Flight-Measured Transients Related to Inlet Performance on the YF-12 Airplane," *Proceedings of YF-12 Experiments Symposium*, NASA CP-2054, vol. III, 1978, pp. 427–473.

[13] Ehernberger, L.J. and Betty J. Love, *High Altitude Gust Acceleration Environment as Experienced by a Supersonic Airplane*, NASA TN D-7868, 1975.

[14] Ehernberger, L.J., "The YF-12 Gust Velocity Measuring System," *Proceedings of YF-12 Experiments Symposium*, NASA CP-2054, vol. I, 1978, pp. 135–154.

[15] Range Commanders Council, *Range Reference Atmosphere, Edwards AFB, California, 0–70 km Altitude*, MG 366-83, 1983.

[16] Ehernberger, L.J., *Atmospheric Conditions Associated With Turbulence Encountered by the XB-70 Airplane Above 40,000 Feet Altitude*, NASA TN D-4768, 1968.

[17] Ball, John T., *Cloud and Synoptic Parameters Associated With Clear Air Turbulence*, NASA CR-111778, 1970.

[18] Incrocci, Thomas P. and James R. Scoggins, *An Investigation of the Relationships Between Mountain-Wave Conditions and Clear Air Turbulence Encountered by the XB-70 Airplane in the Stratosphere*, NASA CR-1878, 1971.

[19] Possiel, Norman and James R. Scoggins, "Curvature of the Wind Profile in the Troposphere Versus Regions of CAT and Non-CAT in the Stratosphere," *Mon. Wea. Rev.*, vol. 104, no. 1, Jan. 1976, pp. 57–62.

[20] Harrison, Henry T., *The Mountain Wave*, NASA CR-315, 1965.

[21] Clark, James W., Richard C. Stoeffler, and Paul G. Vogt, *Research on Instabilities in Atmospheric Flow Systems Associated With Clear Air Turbulence*, NASA CR-1604, 1970.

[22] Dutton, John A. and Hans A. Panofsky, "Clear Air Turbulence—A Mystery May Be Unfolding," *Science*, vol. 167, no. 3920, Feb. 1970, pp. 937–944.

[23] Atlas, D., J.I. Metcalf, J.H. Richter, and E.E. Gossard, "The Birth of 'CAT' and Microscale Turbulence," *J. Atmospheric Sciences*, vol. 27, Sept. 1970, pp. 903–913.

[24] Browning, K.A., A. McPherson, and J.R. Starr, "Simultaneous Measurements of Clear Air Turbulence at the Tropopause by High-Power Radar and Instrumented Aircraft," *Nature*, vol. 228, 1970, pp. 1065–1067.

[25] Metcalf, J.I. and D. Atlas, "Meteorological Structure of Thin Clear Air Scatter Layers Observed by Ultra-High Resolution Radar," *Proceedings of the 15th Radar Meteorology Conference*, Urbana, Oct. 10–12, 1972, pp. 242–274.

[26] Holmboe, Jörgen and Harold Klieforth, *Investigation of Mountain Lee Waves and the Air Flow Over the Sierra Nevada*, AFCRC TR-57-204, 1957.

[27] Lilly, D.K., Y. Pann, P. Kennedy, and W. Toutenhoofd, *Data Catalog for the 1970 Colorado Lee Wave Observation Program*, NCAR-TN/STR-72, 1971.

[28] Lilly, D.K., "Observations of Mountain-Induced Turbulence," *J. Geophys. Res.*, vol. 76, 1971, pp. 6585–6588.

[29] Wurtele, M.G. and A. Datta, "Lee Waves, Benign and Malignant," *Measurement and Modeling of Environmental Flows—1992*, American Society of Mechanical Engineers, New York, 1992, pp. 109–122.

[30] Pihos, Gregory G. and Morton G. Wurtele, *An Efficient Code for the Simulation of Nonhydrostatic Stratified Flow Over Obstacles*}, NASA CR-3385, 1981.

[31] Durran, D.R. and J.B. Klemp, "A Compressible Model for the Simulation of Moist Mountain Waves," *Mon. Wea. Rev.*, vol. 111, 1983, pp. 2341–2361.

[32] Sharman, R.D., T.L. Keller, and M.G. Wurtele, "Incompressible and Anelastic Flow Simulations on Numerically Generated Grids," *Mon. Wea. Rev.*, vol. 116, 1988, pp. 1124–1136.

[33] Kim, Young-Joon and Akio Arakawa, "Assessment of Gravity-Wave Parameterization Schemes Using a Mesoscale Gravity-Wave Model," *Preprints Ninth Conference on Numerical Weather Prediction*, Am. Meteor. Soc., Boston, 1991, pp. 380–383.

[34] Ehernberger, L.J., Dale R. Durran, Peter P. Miller, S. Ward, M.G. Wurtele, R.D. Sharman, A. Datta, Y.J. Kim, T.L. Keller, and Terry L. Clark, Comparison of 2-D Numerical Simulations With Observed Wave and Turbulence Activity in the Lower Stratosphere. (Scheduled for publication as a NASA report in 1993. Forward requests for this document to L.J. Ehernberger.)

[35] Helvey, R.A., *Observations of Stratospheric Clear Air Turbulence and Mountain Waves Over the Sierra Nevada Mountains—An Analysis of the U-2 Flights of 13--14 May 1964*, AFCRL-68-0001, 1967.

[36] Waco, David E., "Temperature Gradients in Stratospheric Turbulence," *J. Appl. Met.*, vol. 11, 1972, pp. 99–107.

[37] Nicholls, J.M., "Measurements of Stratospheric Airflow and Clear Air Turbulence, up to 63,000 ft, Over and Downwind of Mountainous Terrain," *Proceedings of RAeS/CASI/AIAA International Conference on Atmospheric Turbulence*, London, 1971.

[38] Hines, C.O., "Internal Atmospheric Gravity Waves at Ionospheric Heights," *Canadian J. Phys.*, vol. 38, 1960, pp. 1441–1481.

[39] Fritts, D.C., "Gravity Wave Saturation in the Middle Atmosphere: A Review of Theory and Observations," *Rev. Geophys. Space Phys.*, vol. 22, 1984, pp. 275–308.

[40] Philbrick, C.R. and B. Chen, "Transmission of Gravity Waves and Planetary Waves in the Middle Atmosphere Based on Lidar and Rocket Measurements," *Adv. Space Res.*, vol. 12, no. 10, 1992, pp. (10)303–(10)306.

[41] Fetzer, E.J., *A Global Climatology of Middle Atmosphere Inertia-Gravity Waves*, Ph.D. Thesis, U. of Colorado, 1990.

[42] Findlay, J.T., S.P. Berube, and G.D. Qualls, *Shuttle-Derived Density Profiles in the Middle Atmosphere*, NASA CR-4109, 1988.

[43] Bacmeister, J.T. and M.R. Schoeberl, "Breakdown of Vertically Propagating Two-Dimensional Gravity Waves Forced by Orography," *J. Atmos. Sci.*, vol. 46, no. 14, 1989, pp. 2109–2134.

[44] Landau, D.M. and M.G. Wurtele, Resonant Backscattering of a Gravity Wave From a Critical Level, *Proceedings of Eighth Conference of Atmospheric and Oceanic Waves and Stability*, Am. Meteor. Soc., Boston, 1991, pp. 244–247.

[45] Datta, A., *Propagation of Gravity, Inertia-Gravity, and Lee Waves in Two Dimensions*, M.S. Thesis, U. of California, Los Angeles, 1991.

[46] Keller, T.L., M.G. Wurtele, and R.D. Sharman, "Implications of the Hydrostatic Assumption on Atmospheric Gravity Waves," *Proceedings of Eighth Conference of Atmospheric and Oceanic Waves and Stability*, Am. Metero. Soc., Boston, 1991, pp. 320–323.

[47] Wingrove, R.C., R.E. Bach, Jr., and T.A. Schultz, "Analysis of Severe Atmospheric Disturbances From Airline Flight Records," *Flight in Adverse Environmental Conditions*, AGARD CP-470, 1989, pp. 3-1 to 3-7.

[48] Schweikhard, W.G., G.B. Gilyard, J.E. Talbot, and T.W. Brown, *Effects of Atmospheric Conditions on the Operating Characteristics of Supersonic Cruise Aircraft*, Presented at XXVII Congress of the International Astronautical Federation (I.A.F.), Anaheim, California, I.A.F. 76-112, Oct. 16, 1976.

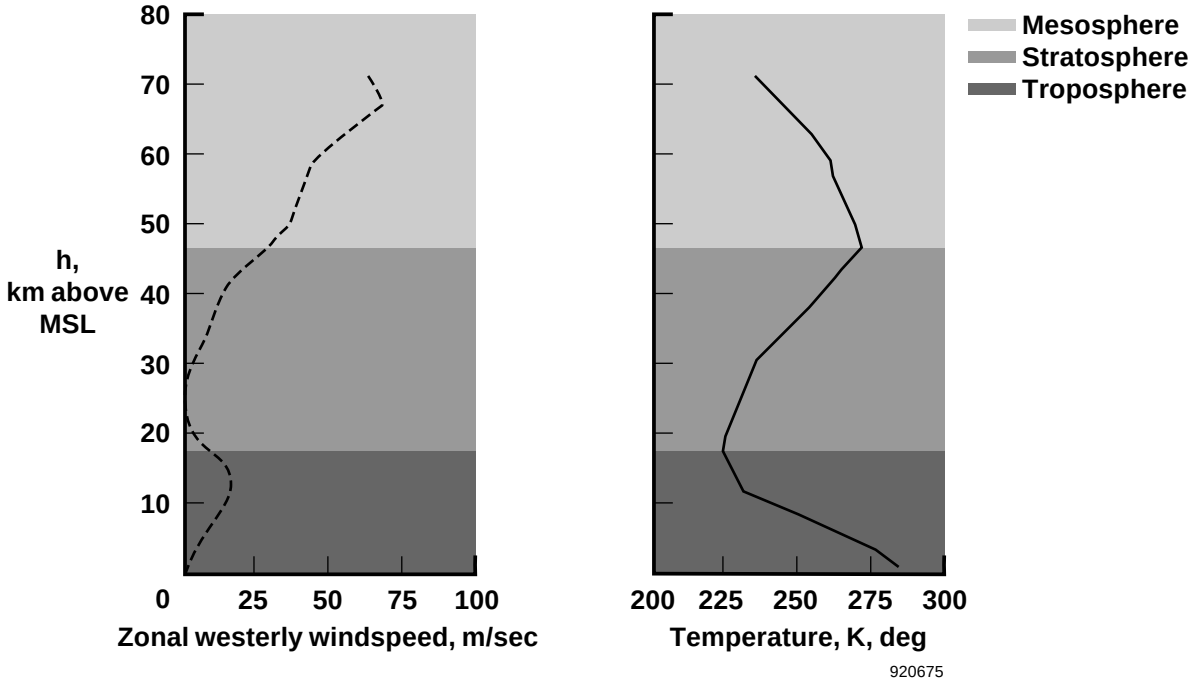

Fig. 1 Representative atmospheric structure, January average for Edwards, California (Ref. 15).

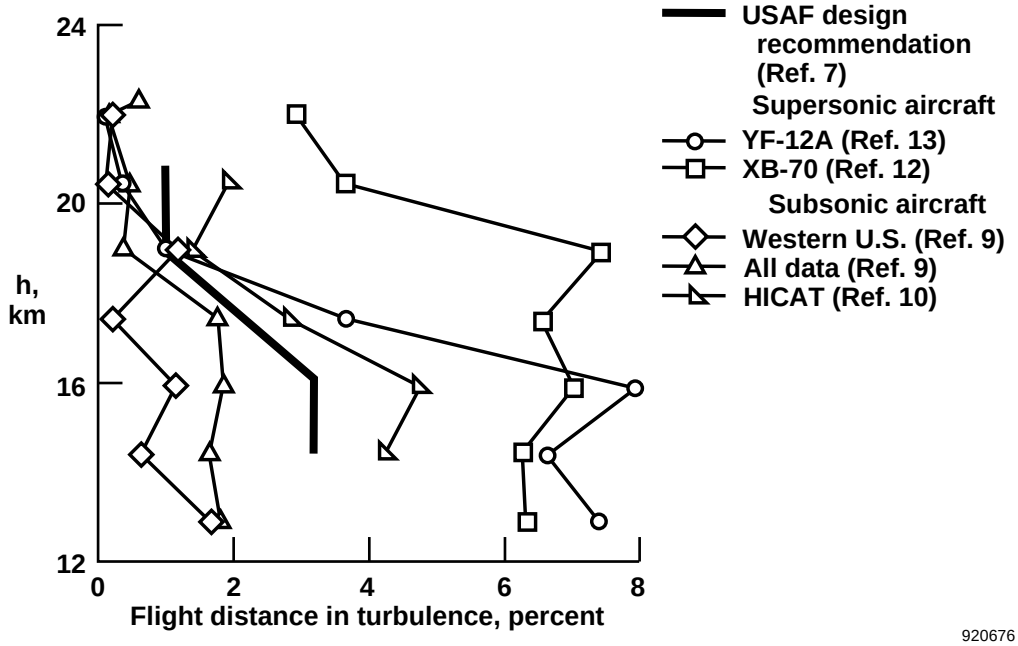

Fig. 2 High-altitude turbulence survey results for amount of turbulence expressed as the percent of flight distance (Ref. 13).

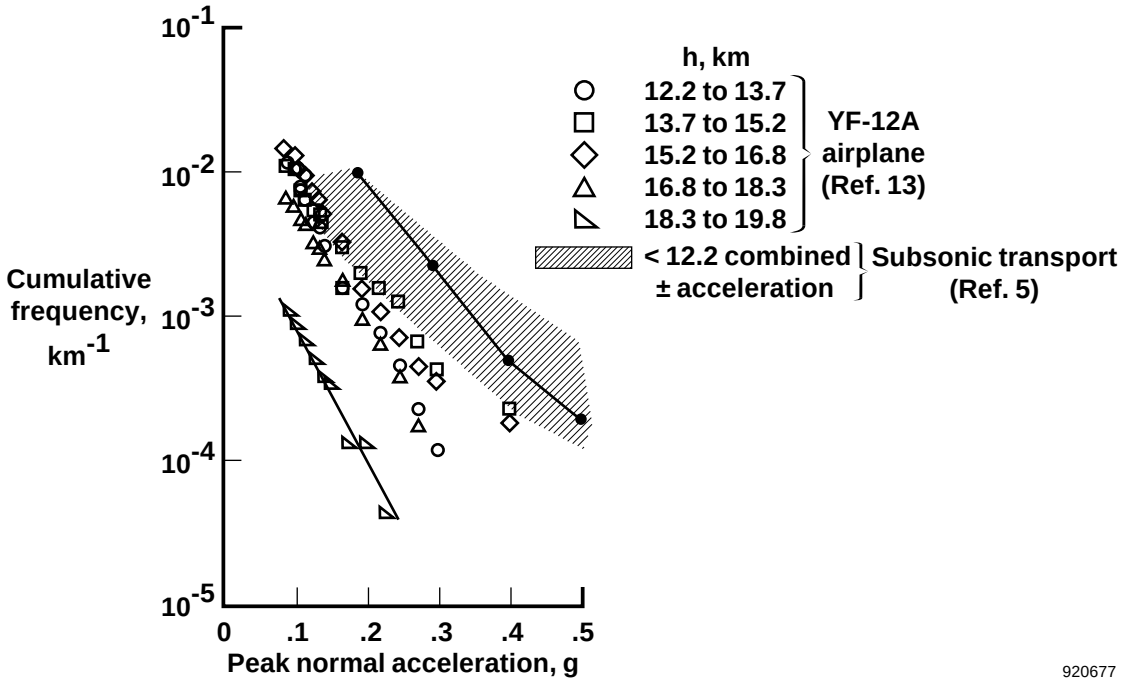

Fig. 3 Cumulative frequency distributions of peak accelerations caused by turbulence.

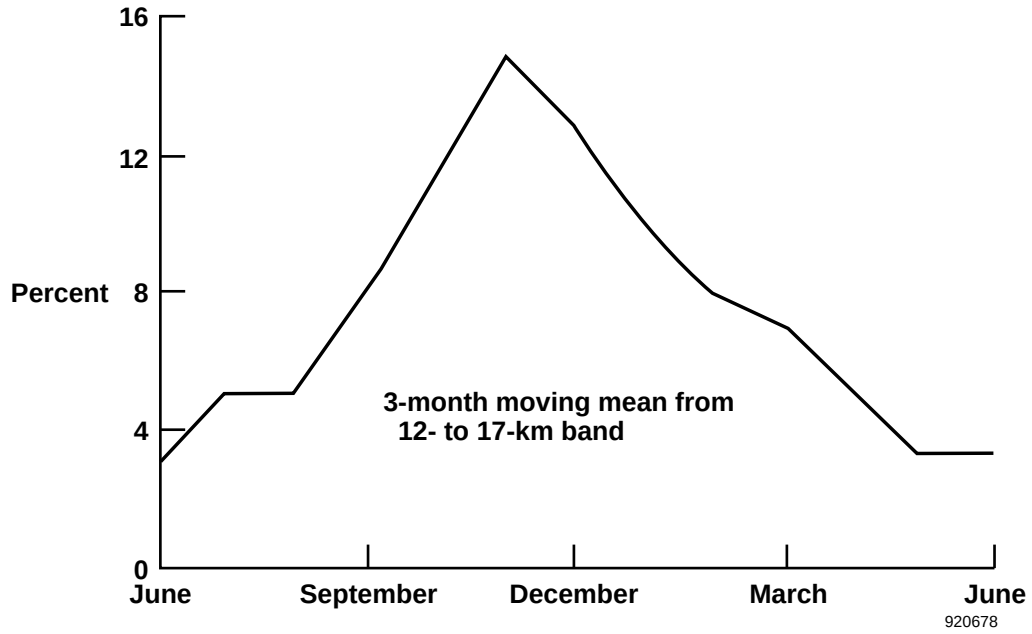

Fig. 4 Seasonal variation of turbulence encountered in the lower stratosphere between 12 and 17 km.

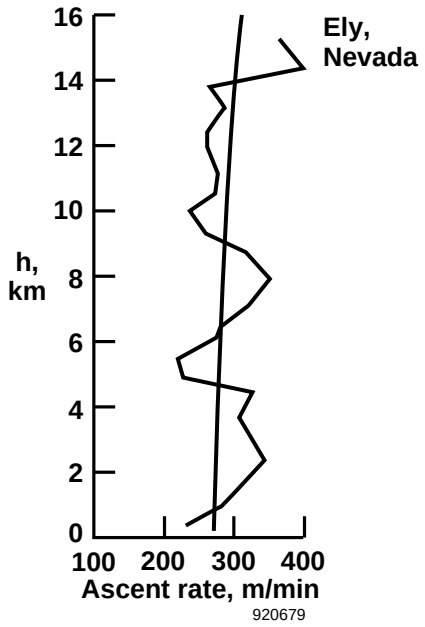

(a) Rate variations of 50 to 150 m/min for turbulence near Ely, Nevada.

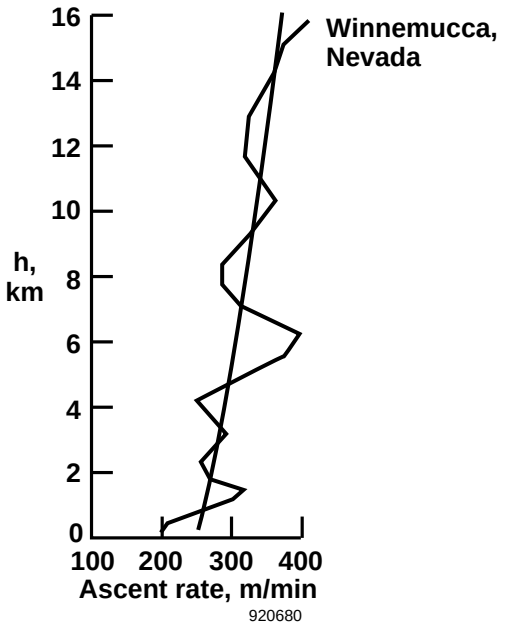

(b) Rate variations of 50 to 150 m/min for turbulence near Winnemucca, Nevada.

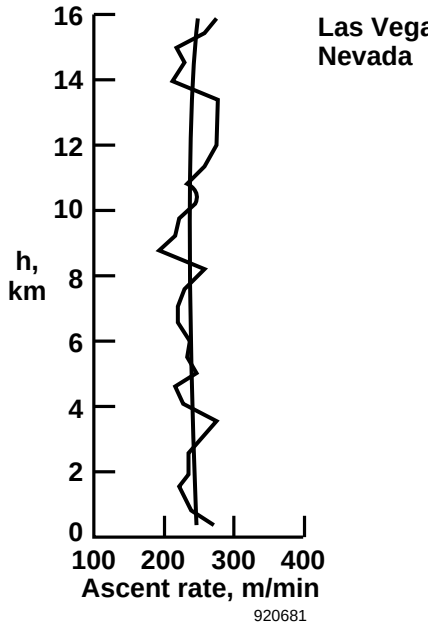

(c) Rate variations of 30 to 70 m/min for nonturbulence near Las Vegas, Nevada.

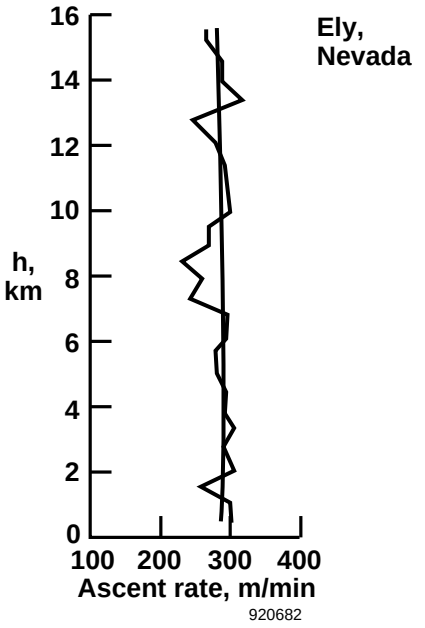

(d) Rate variations of 30 to 70 m/min for nonturbulence near Ely, Nevada.

Fig. 5 Rawinsonde balloon ascent rate profiles for turbulence and nonturbulence areas encountered in high-altitude supersonic flight (Ref. 18).

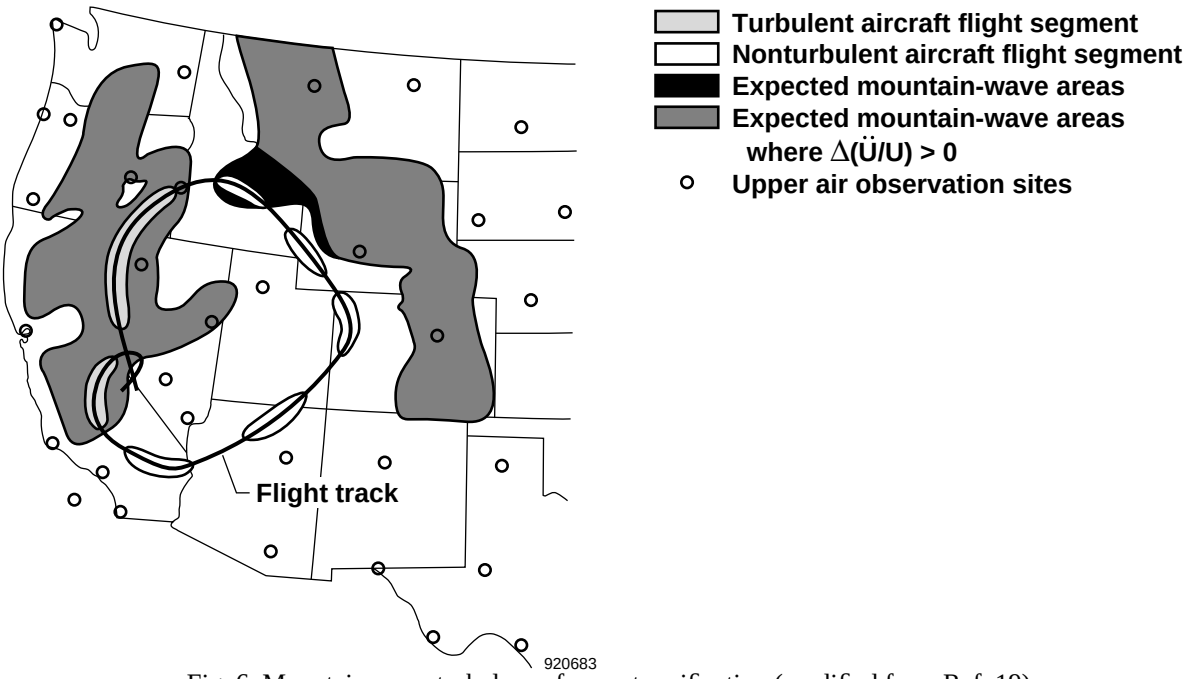

Fig. 6 Mountain-wave turbulence forecast verification (modified from Ref. 19).

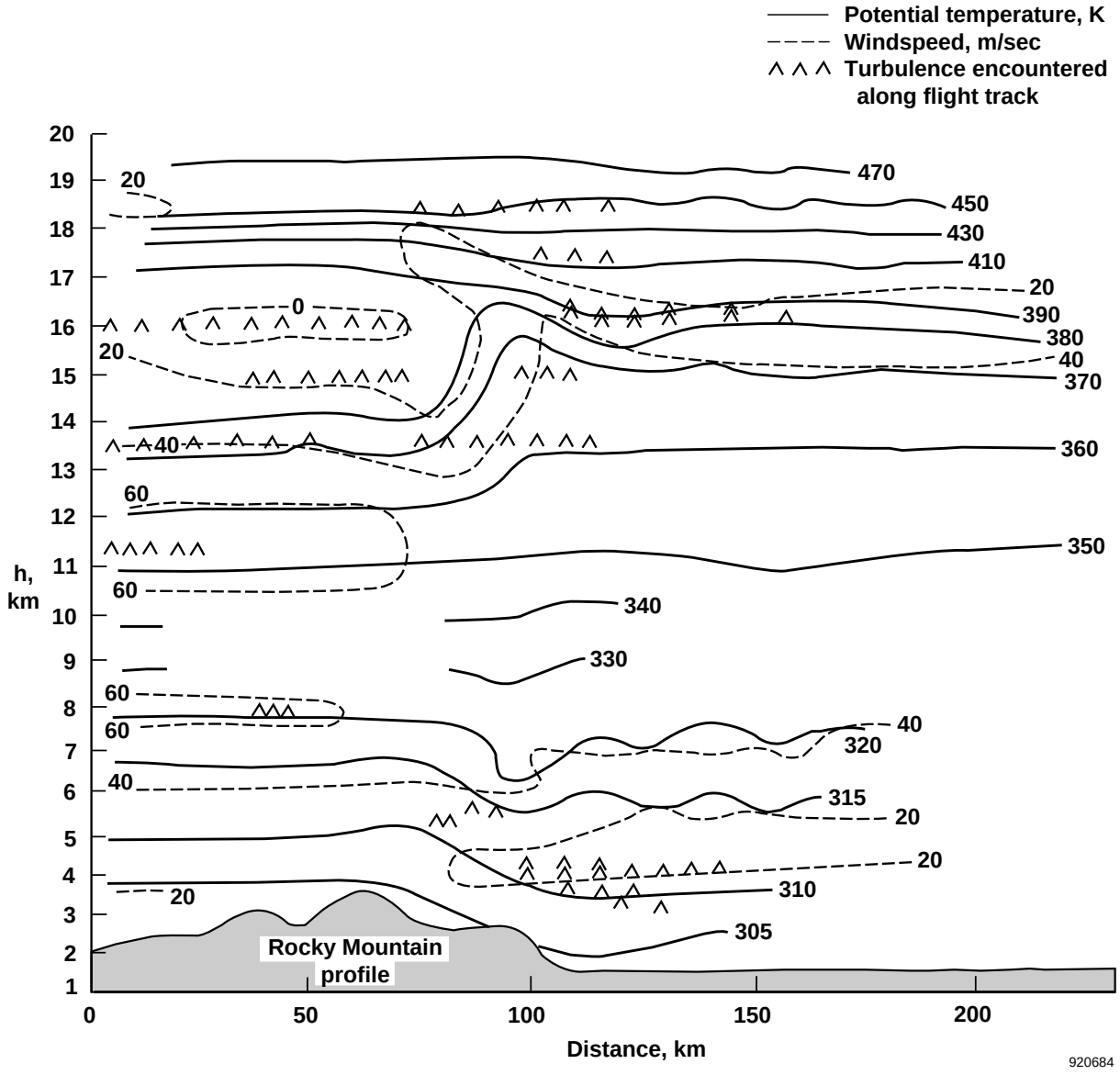

Fig. 7 Cross-section of potential temperature and windspeed analyzed from in-situ aircraft data for mountain-wave turbulence (Ref. 28).

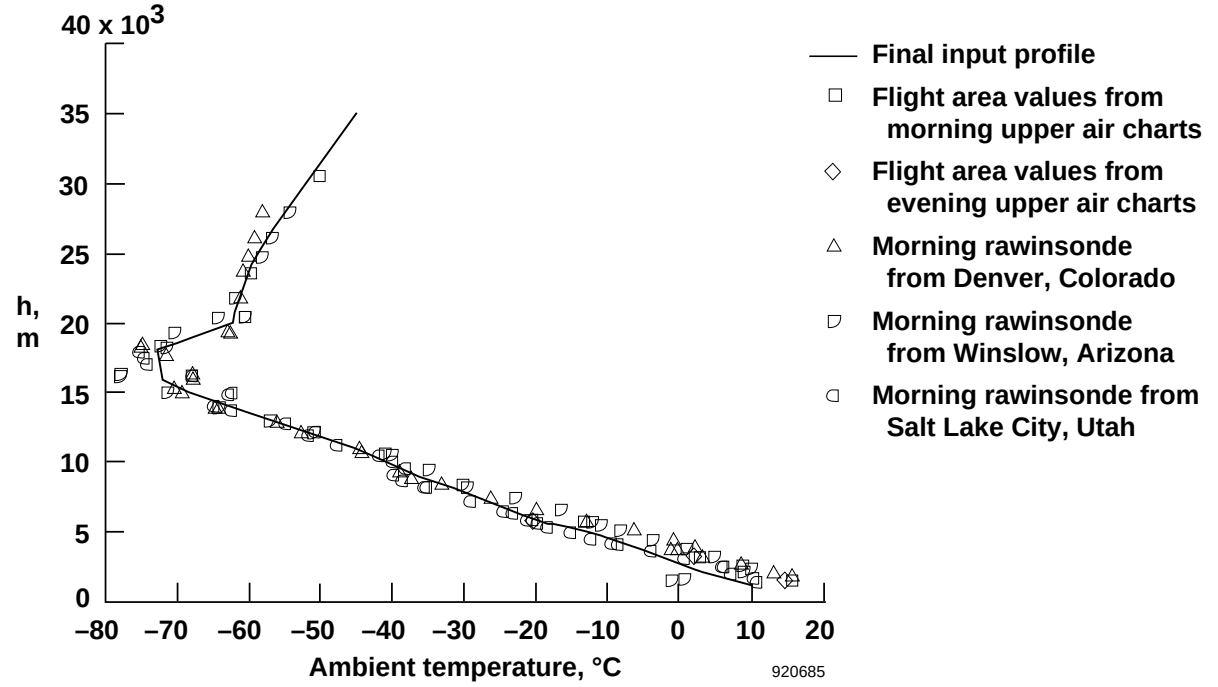

Fig. 8 Input temperature profile and rawinsonde observation data for simulation of mountain-wave turbulence in the stratosphere.

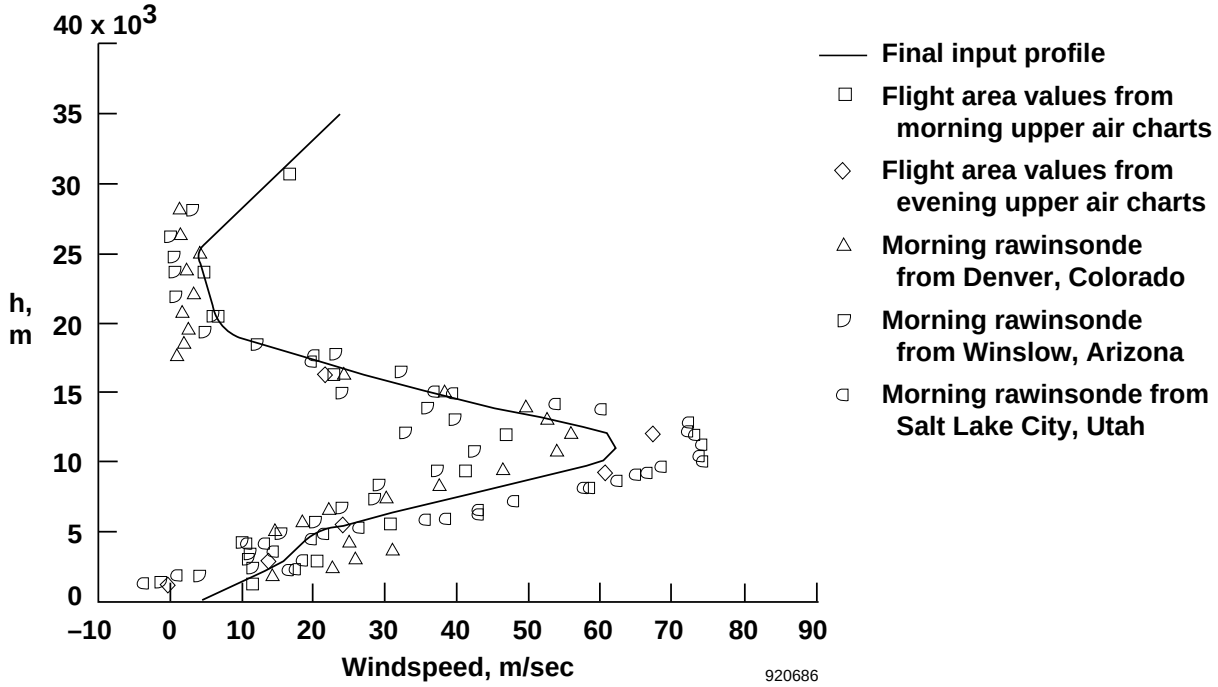

Fig. 9 Input wind profile and rawinsonde observation data for mountain-wave turbulence in the stratosphere.

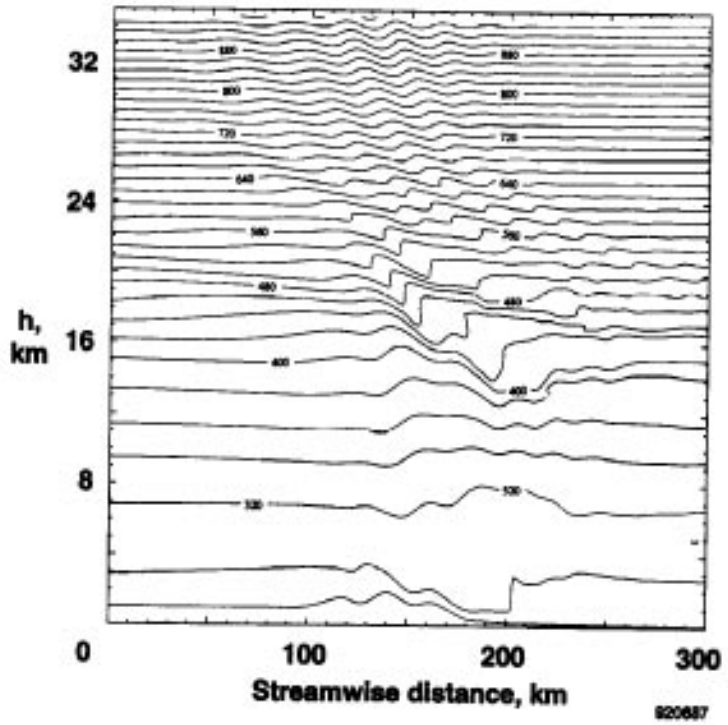

(a) Potential temperature contours (K, deg) for strong turbulence.

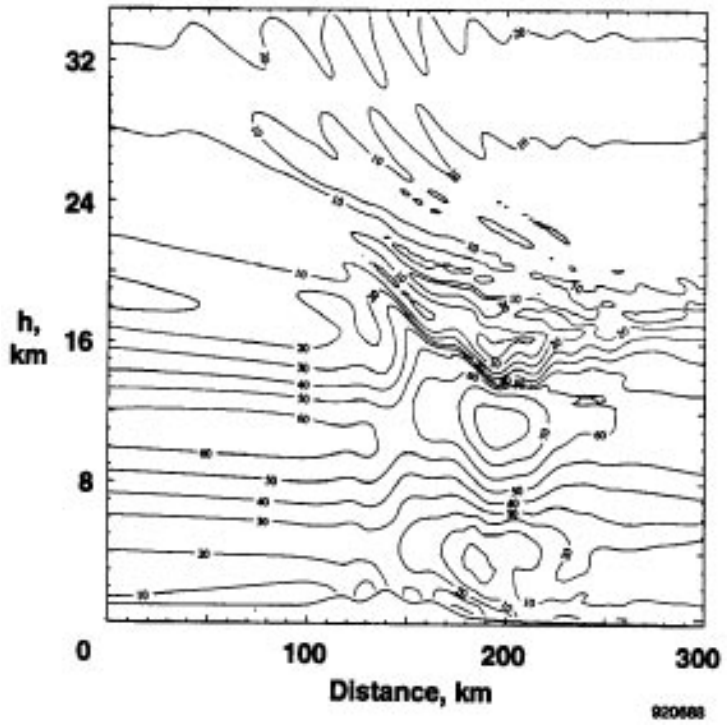

(b) Horizontal velocity contours (m/sec) for strong turbulence.

Fig. 10 Vertical and horizontal cross-sections for numerical simulations of potential temperature and wind contours with and without observed turbulence in the stratosphere.

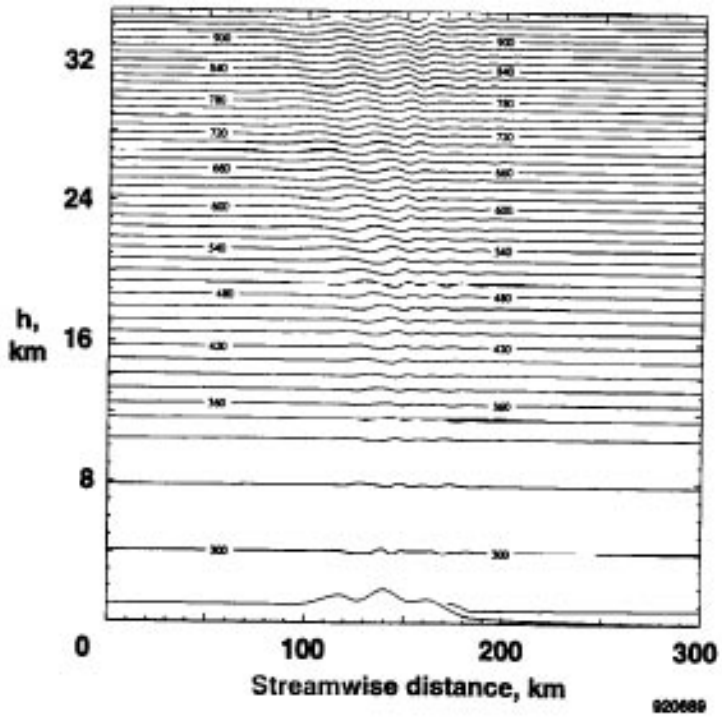

(c) Potential temperature contours (K, deg) without turbulence.

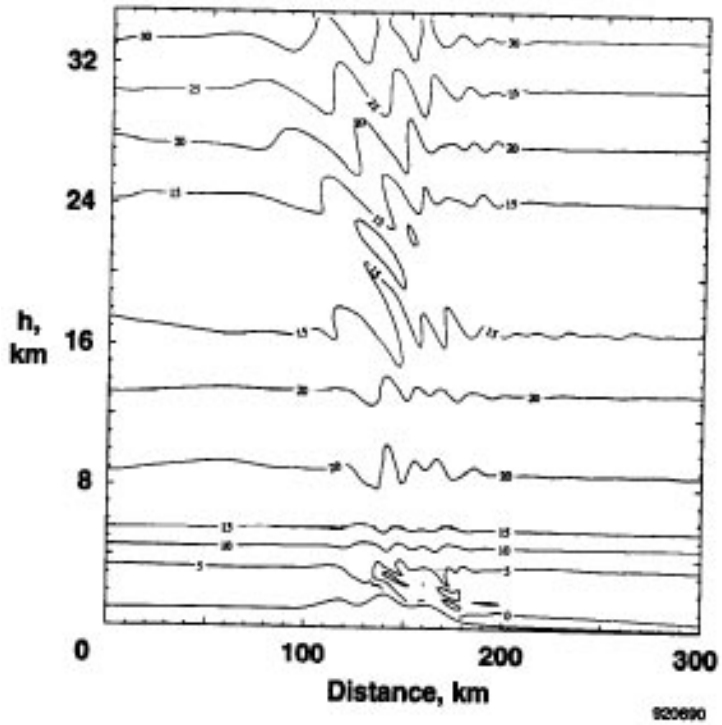

(d) Horizontal velocity contours (m/sec) without turbulence.

Fig. 10 Concluded.

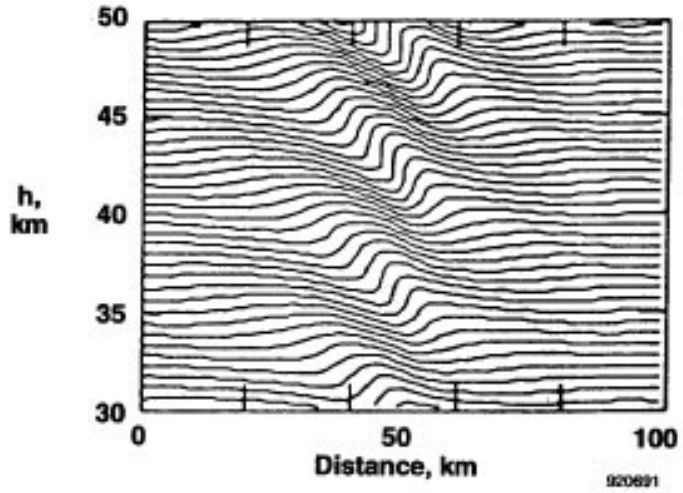

(a) Waves steepen, 10 hr.

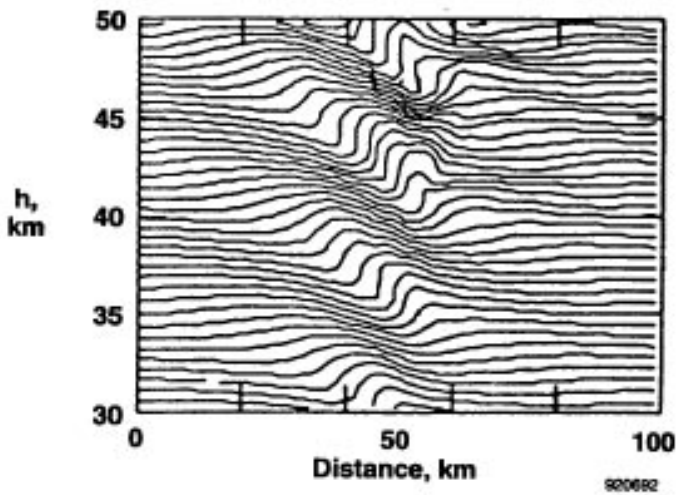

(b) Waves breaking and overturning, 12 hr.

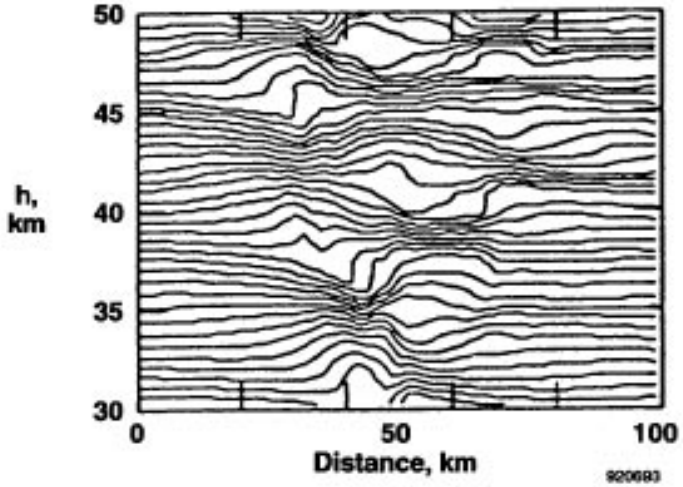

(c) Well-developed turbulence regions, 14 hr.

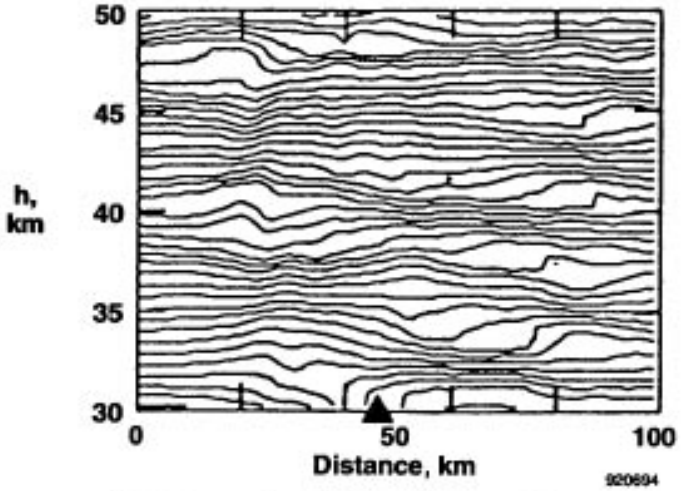

(d) Waves and turbulence decay, 16 hr.

Fig. 11 Numerical simulation of wave amplitude growth, breakdown and overturning, instability, and decay in the upper stratosphere (Ref. 43).

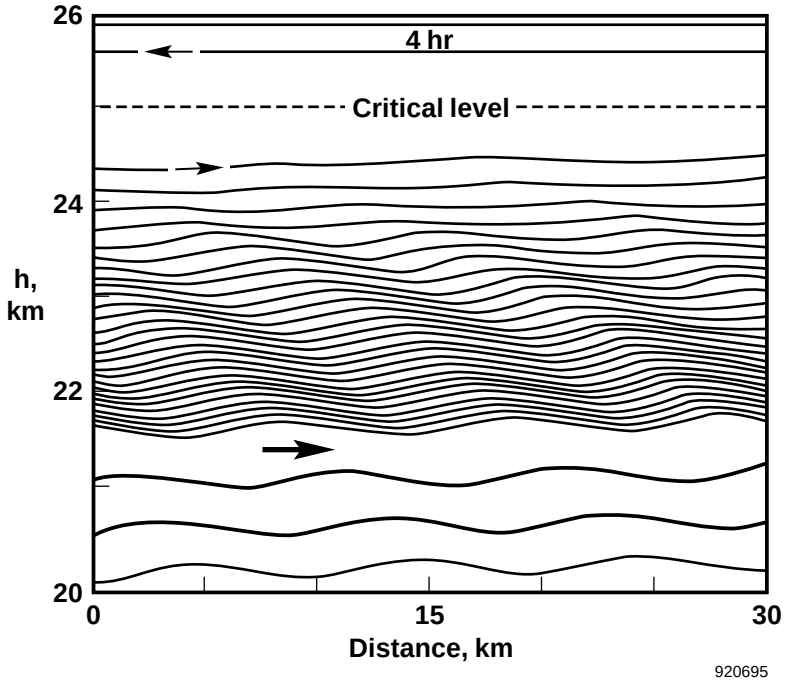

(a) At 4 hr, monotonic wave upward propagation approaches the critical level at 25 km.

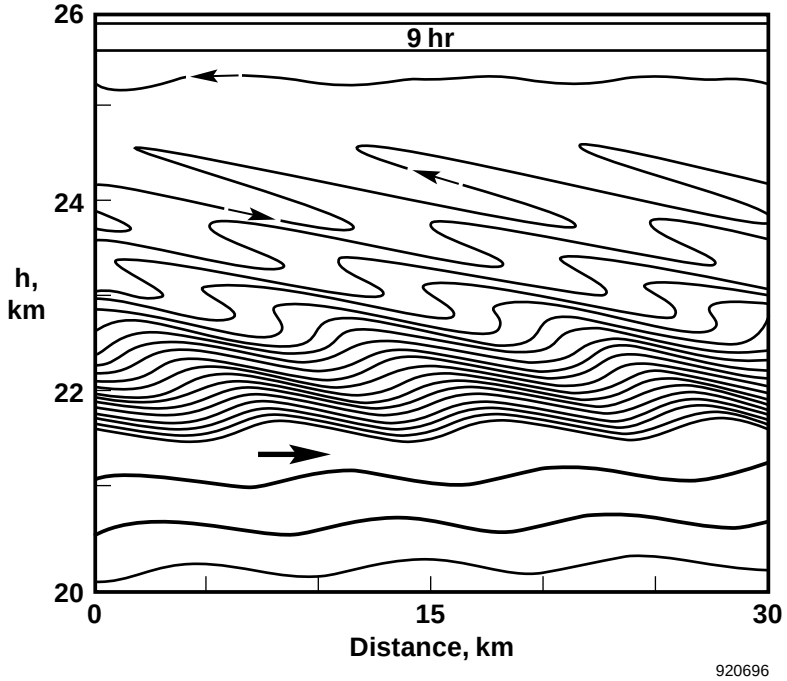

(b) At 9 hr, critical level interaction induces zones of reverse flow between 22.5 and 25 km.

Fig. 12 Numerical simulation streamfunction field showing instability development beneath the critical level at 25 km resulting from upward propagation of a monotonic wave at an altitude of 15 km (Ref. 44).

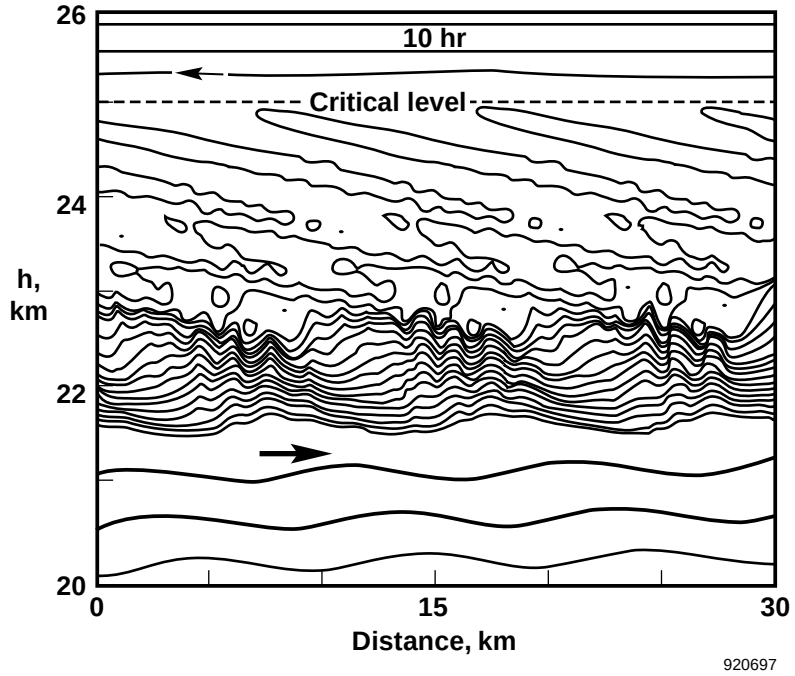

(c) At 10 hr, smaller scale perturbations develop.

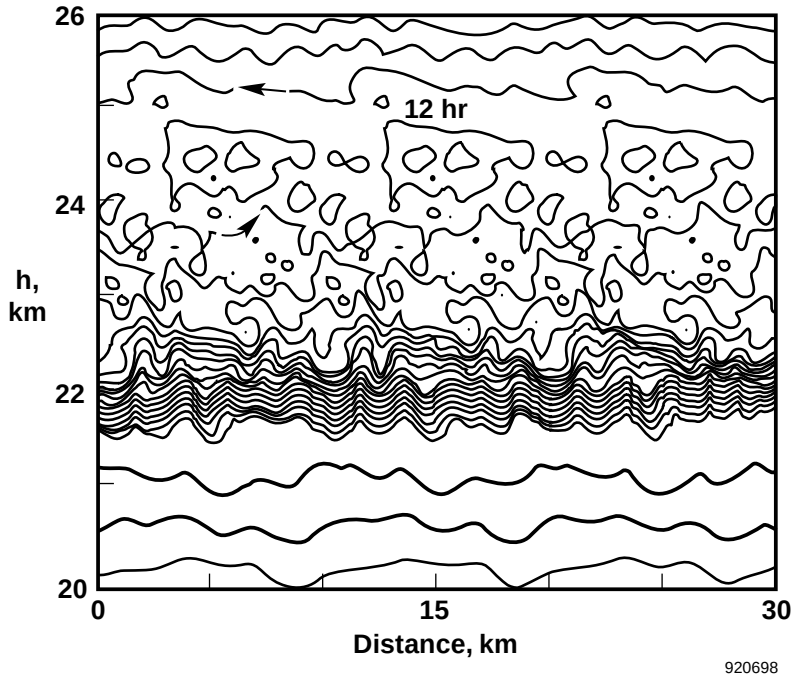

(d) At 12 hr, perturbations have developed at smaller scales and propagate to both higher and lower altitudes.

Fig. 12 Concluded.

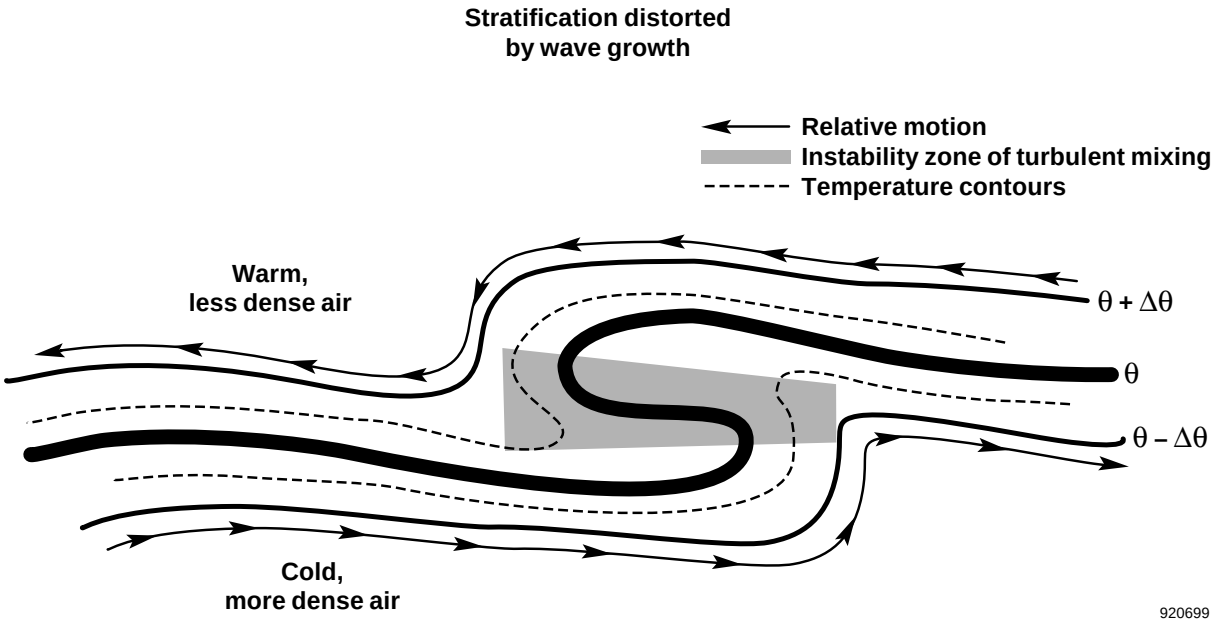

Fig. 13 Schematic of distorted atmospheric potential temperature stratification leading to instability and vortex wrap up.

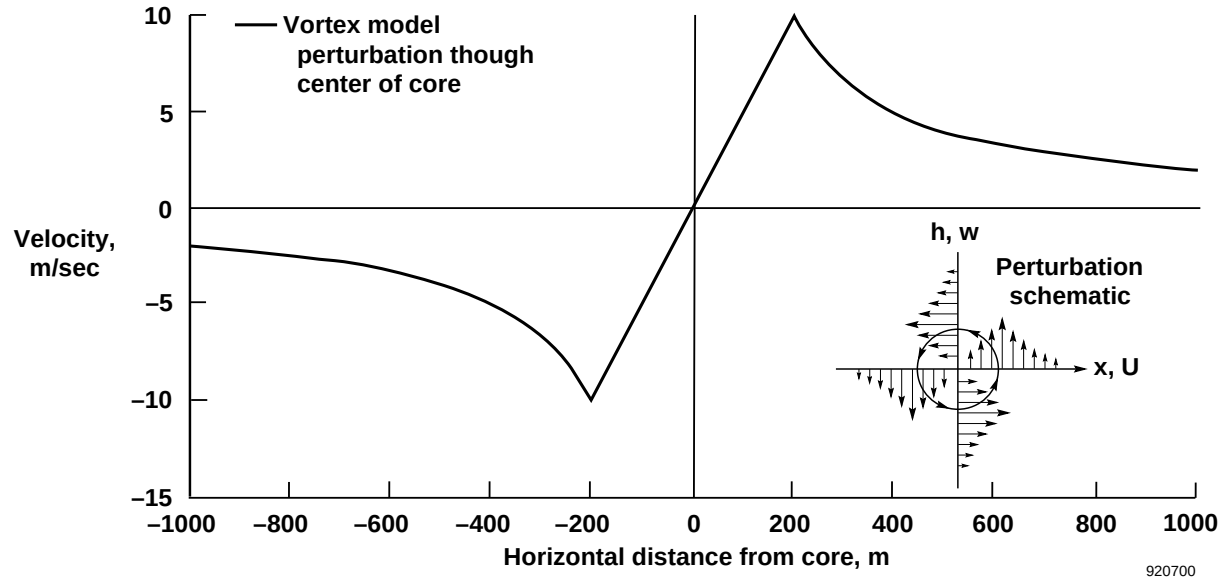

(a) Vertical component for horizontal trajectory through the core center.

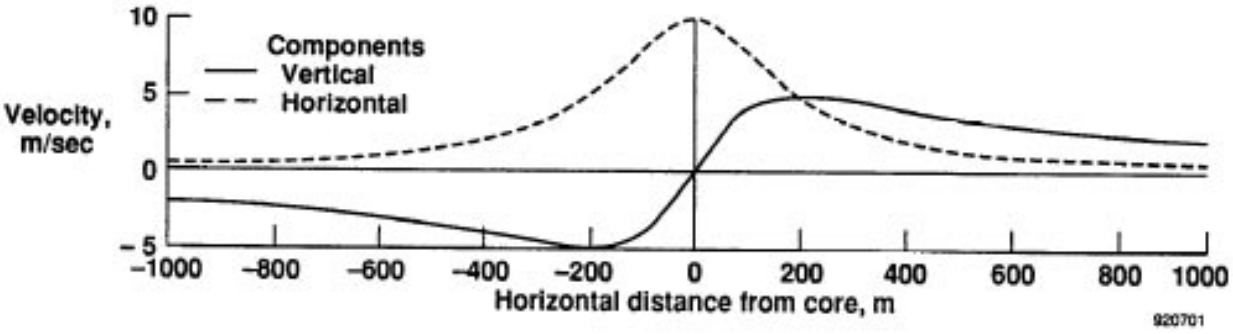

(b) Components for a trajectory through the core top.

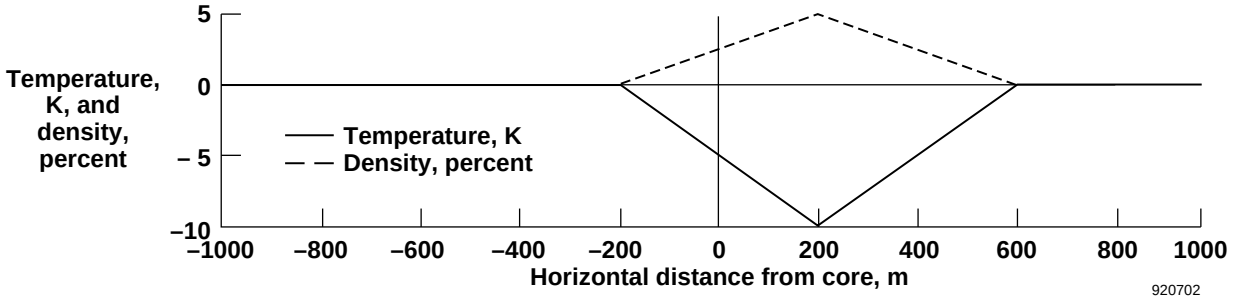

(c) Thermodynamic perturbations for a trajectory through the core top.

Fig. 14 Discrete, small-scale, two-dimensional, atmospheric perturbation model.

REPORT DOCUMENTATION PAGE

Form Approved
OMB No. 0704-0188

1. AGENCY USE ONLY (Leave blank)	2. REPORT DATE	3. REPORT TYPE AND DATES COVERED
	December 1992	Technical Memorandum

4. TITLE AND SUBTITLE

Stratospheric Turbulence Measurements and models for Aerospace Plane Design

5. FUNDING NUMBERS

WU 763-21-51

6. AUTHOR(S)

L.J. Ehernberger

7. PERFORMING ORGANIZATION NAME(S) AND ADDRESS(ES)

NASA Dryden Flight Research Facility
P.O. Box 273
Edwards, California 93523-0273

8. PERFORMING ORGANIZATION REPORT NUMBER

H-1865

9. SPONSORING/MONITORING AGENCY NAME(S) AND ADDRESS(ES)

National Aeronautics and Space Administration
Washington, DC 20546-0001

10. SPONSORING/MONITORING AGENCY REPORT NUMBER

NASA TM-104262

11. SUPPLEMENTARY NOTES

Presented at the AIAA Fourth International Aerospace Planes Conference, December 1–4, 1992, Orlando, Florida.

12a. DISTRIBUTION/AVAILABILITY STATEMENT

Unclassified—Unlimited
Subject Category 47

12b. DISTRIBUTION CODE

13. ABSTRACT (Maximum 200 words)

Progress in computational atmospheric dynamics is exhibiting the ability of numerical simulation to describe instability processes associated with turbulence observed at altitudes between 15 and 25 km in the lower stratosphere. As these numerical simulation tools mature, they can be used to extend estimates of atmospheric perturbations from the present gust database for airplane design at altitudes below 15 km to altitudes between 25 and 50 km where aerospace plane operation would be at hypersonic speeds. The amount of available gust data and number of temperature perturbation observations are limited at altitudes between 15 and 25 km. On the other hand, in-situ gust data at higher altitudes are virtually nonexistent. The uncertain potential for future airbreathing hypersonic flight research vehicles to encounter strong turbulence at higher altitudes could penalize the design of these vehicles by undue cost or limitations on performance. Because the atmospheric structure changes markedly with altitude, direct extrapolation of gust magnitudes and encounter probabilities to the higher flight altitudes is not advisable. This paper presents a brief review of turbulence characteristics observed in the lower stratosphere and highlights the progress of computational atmospheric dynamics that may be used to estimate the severity of atmospheric transients at higher altitudes.

14. SUBJECT TERMS

Clear air turbulence; Discrete gust models; Hypersonic aircraft; Mountain waves; Numerical simulations; Stratosphere

15. NUMBER OF PAGES

29

16. PRICE CODE

A03

17. SECURITY CLASSIFICATION OF REPORT	18. SECURITY CLASSIFICATION OF THIS PAGE	19. SECURITY CLASSIFICATION OF ABSTRACT	20. LIMITATION OF ABSTRACT
Unclassified	Unclassified	Unclassified	Unlimited